JOURNAL OF PROPULSION AND POWER
Vol. 13, No. 4, July–August 1997

Turbulent Mixing of Coaxial Nozzle Flows with a Central-Lobed Mixer

S. C. M. Yu* and X. G. Xu†
Nanyang Technological University, Singapore 639798, Singapore

The turbulent mixing of turbulent, confined, coaxial nozzle flows with a central-lobed mixer were determined by measurement using a two-component fiber-optic laser Doppler anemometer at a Reynolds number of 5.1×10^4 (based on an inner circular nozzle diameter D_i = 30 mm and bulk mean velocity U_r of the two streams at 1.7 m/s). The ratio of the annular mean to the core mean velocity was 2:1. The boundary-layer thicknesses in the nozzle exit plane were about 3% of the inner circular nozzle diameter. Altogether, three central-lobed mixer configurations were tested, including four-, five-, and six-lobed nozzles. A blunt leading-edge circular central nozzle (i.e., a coaxial jet arrangement) was also measured as a basis for comparison. The results showed that the streamwise vorticity originated from two sources: the geometry of the lobe and the gap between the lobe nozzle peaks and the inner annular wall. The former result was important to enhance the mixing between the two coflowing streams, whereas the latter result was important to the mixing between the annular flow and the surrounding still fluid. No streamwise vorticity would be generated if the size of the gap was larger than 15% of the inner circular nozzle diameter. Furthermore, when flow separation appeared at the lobe peaks, the strength of the streamwise vorticity generated by the gap would be strengthened with a consequence of enhancing the mixing between the annular flow and the surrounding still fluid; the number of the lobes also played an important role in the mixing processes. A center plug was found to be effective in enhancing the mixing between the two coflowing streams by eliminating the flow separation at the lobe peak regions for the six-lobed case, but with a consequence of suppressing the streamwise vorticity generated by the gap.

Nomenclature

D_i = inner circular nozzle diameter at 30 mm
D_o = annular nozzle diameter at 60 mm
H = boundary-layer shape factor, δ^*/Θ
k = turbulent kinetic energy, $\frac{1}{2}(u'^2 + v_r'^2 + v_\theta'^2)$
$\dot{m}$ = integrated mass flux at different streamwise stations downstream of the trailing edge
$\dot{m}_e$ = integrated mass flux at the exit plane of the coaxial nozzle
Re = Reynolds number, $U_r D_i/\upsilon$, 5.1×10^4
Re_Θ = Reynolds number based on the momentum thickness
U_r = bulk mean velocity for the two streams, 1.7 m/s
U_s = secondary mean velocity, $\sqrt{V_r^2 + V_\theta^2}$
U, u' = streamwise mean and the corresponding rms velocities
$\overline{u'v_r'}$, $\overline{u'v_\theta'}$ = Reynolds shear stresses
V_r, v_r' = radial mean and the corresponding rms velocities
V_θ, v_θ' = circumferential mean and the corresponding rms velocities
x, r, θ = streamwise, radial, and circumferential directions, in a polar coordinate system
x, y, z = streamwise, horizontal, and vertical directions, in a Cartesian coordinate system
δ^* = displacement thickness, mm
Θ = momentum thickness, mm
υ = kinematic viscosity
Ω_x = streamwise vorticity, $(\partial V_r/r\partial\theta) - (\partial V_\theta/\partial r)$
$\Omega_{x,\text{peak}}$ = peak streamwise vorticity

Received Aug. 7, 1996; revision received March 26, 1997; accepted for publication March 26, 1997.

*Senior Lecturer, Thermal and Fluids Engineering Division, School of Mechanical and Production Engineering. Member AIAA.

†Graduate Student, Thermal and Fluids Engineering Division, School of Mechanical and Production Engineering.

I. Introduction

THE flow behavior of coaxial jets is of great interest because of their relevance in many industrial applications: for example, industrial burners, ejectors, and turbofan engine exhausts. Ribeiro and Whitelaw[1,2] studied the mixing between the coaxial flows, both confined and unconfined, through extensive hot-wire and laser Doppler anemometry (LDA) measurements with fully developed initial conditions. Velocity measurements with thin initial boundary layers were also conducted by Champagne and Wygnanski,[3] Ko and Kwan,[4] and Kwan and Ko[5] with various velocity ratios across the jet. One of the major conclusions reached from the aforementioned research works is that the flow discharged from a coaxial jet can actually achieve a self-preserving state at a much faster rate than a single jet, and intense mixing between the coflowing streams is largely a result of the presence of the spanwise vorticity at the inner nozzle wall originated from the Kelvin–Helmholtz instability.

It was determined that the introduction of streamwise vorticity should further enhance the mixing between the two streams. Streamwise vorticity can be introduced by many methods, for example, by installing small vortex generators or tabs immediately upstream of the trailing edge or having a corrugated trailing-edge profile for the inner jet, i.e., a lobed forced mixer.

Application of lobed mixers in the turbofan engine exhausts and ejectors have been studied extensively in the past.[6–10] The rapid mixing of the core and the bypass flows can actually achieve noise reduction and thrust augmentation. The lobe shape and the lobe penetration angle were the important parameters to determine the effectiveness of mixer performance. The streamwise vorticities were essentially inviscidly generated and their strength would be higher when the lobe penetration region consisted of straight parallel sidewalls.

Almost all of the subsequent investigations in lobed forced mixer flows were obtained in a two-dimensional flow situation where the lobed forced mixer was represented by a splitter plate with a corrugated trailing edge (Fig. 1). The water-tunnel visualization tests[6] revealed that both the streamwise vorticity and the accompanying increase in initial interfacial area (relative to a flat plate) were significant contributors to the mixing enhancement of forced lobed mixers. The structure of the flow behind the lobed mixer followed a three-step process, by which the streamwise vortex cells were formed, intensified, and then broken down. The most intense mixing seemed to occur at the third region. Varying the velocity ratio across the lobe could cause a shift in the locations of these three regions.

Velocity measurements by McCormick and Bennett[7] and Yu and Yip[8] concluded that intense small-scale turbulence and mixing occurred at about two to four wavelengths downstream (of the trailing-edge lobe shape) of the mixer trailing edge and were caused mainly by the deformation of the spanwise vortex into a pinched-off structure by the streamwise vortices. At a higher velocity ratio, the spanwise vortex would in turn deform the streamwise vortices of alternative signs (within a lobe) into another pinched-off structure, causing their mutual annihilation.[8] The decay length for the streamwise vorticity from the trailing edge can also be considered a good indication for complete mixing.[9]

Although the results obtained from the experiments of a two-stream mixing flow situation reveal many important mixing characteristics of the forced mixers, many practical applications of the lobed mixer are in the form of the coaxial nozzle, where the flows considered should also include the mixing with the surrounding stagnant environment. Furthermore, when a two-dimensional lobed mixer plate is being used, the vertical components of the secondary flow velocities would be higher than the horizontal components, whereas they would become comparable in a three-dimensional situation, as shown in the measurements of Belovich and Samimy.[10] The effects of higher secondary flow velocities could be significant to the overall flowfield development.

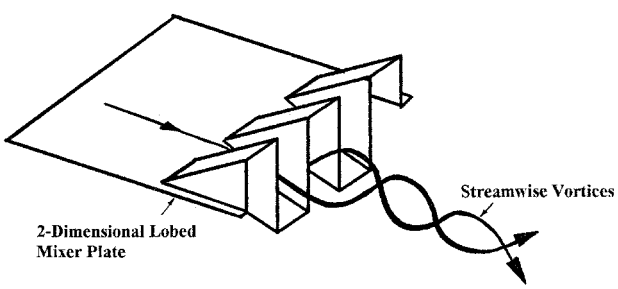

Fig. 1 Two-dimensional lobed forced mixer.

Detailed velocity measurements obtained in a lobed mixer nozzle flow environment appear to be very scarce. Only the measurements of Belovich and Samimy[10] are known to the authors. Thus, the objectives of the present study are twofold. The first objective's goal is to study the downstream evolution of the streamwise vortex structure, while the second objective is to provide detailed velocity measurements suitable for a critical assessment of different turbulence models proposed to predict this type of industrial flow.

Velocity ratios (outer to inner) less than 1 are more relevant to certain types of combustion and turbofan exhaust systems than those greater than 1. Hence, a coaxial nozzle with a velocity ratio of 2:1 (outer to inner), was generated with initial thin turbulent boundary layers. The effects of different velocity ratios across the lobe will be presented in a future communication.[11]

The following section describes briefly the experimental setups including the LDA for obtaining velocity measurements. It will be followed by presentation and discussion of the results. This paper ends with a summary of important findings.

II. Flow Configurations and Instrumentation

A. Wind Tunnel

The water-tunnel facility used in the present investigation is shown schematically in Fig. 2. Water is delivered to a setting chamber through a centrifugal pump with a control valve at the outlet to monitor the flow rate. A coaxial contraction cone of area ratio 10:1 (for both the inner and outer cones) accelerates the flow before discharging into a transparent rectangular test section of 400 × 400 × 1000 mm. The outlet of the jet is extended into the test section by 60 mm. Velocity difference between the inner and outer nozzles is achieved by incorporating screens and wire meshes at the central nozzle so that a ratio of 2:1 (outer to inner) could be achieved. The flow passes through the transparent test section and settles at the sump tank (1000 × 1000 × 1000 mm) located at the back of the test section. Further details of the water tunnel design can be found in Ref. 12.

B. Lobed Nozzle Configurations

Three central-lobed mixer configurations and one baseline circular nozzle have been tested. Figure 3 provides the detailed

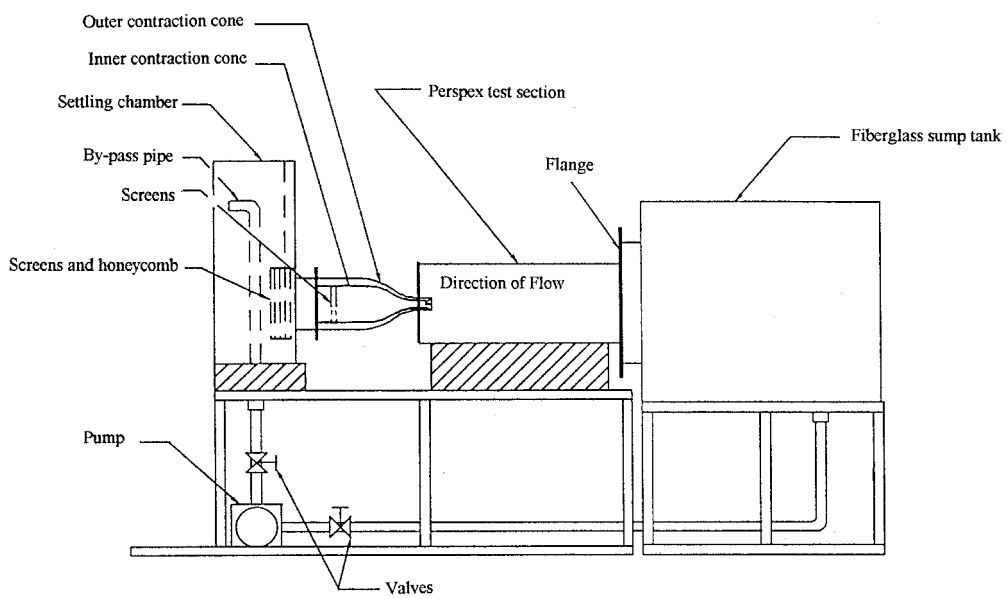

Fig. 2 Schematic of the water-tunnel facilities.

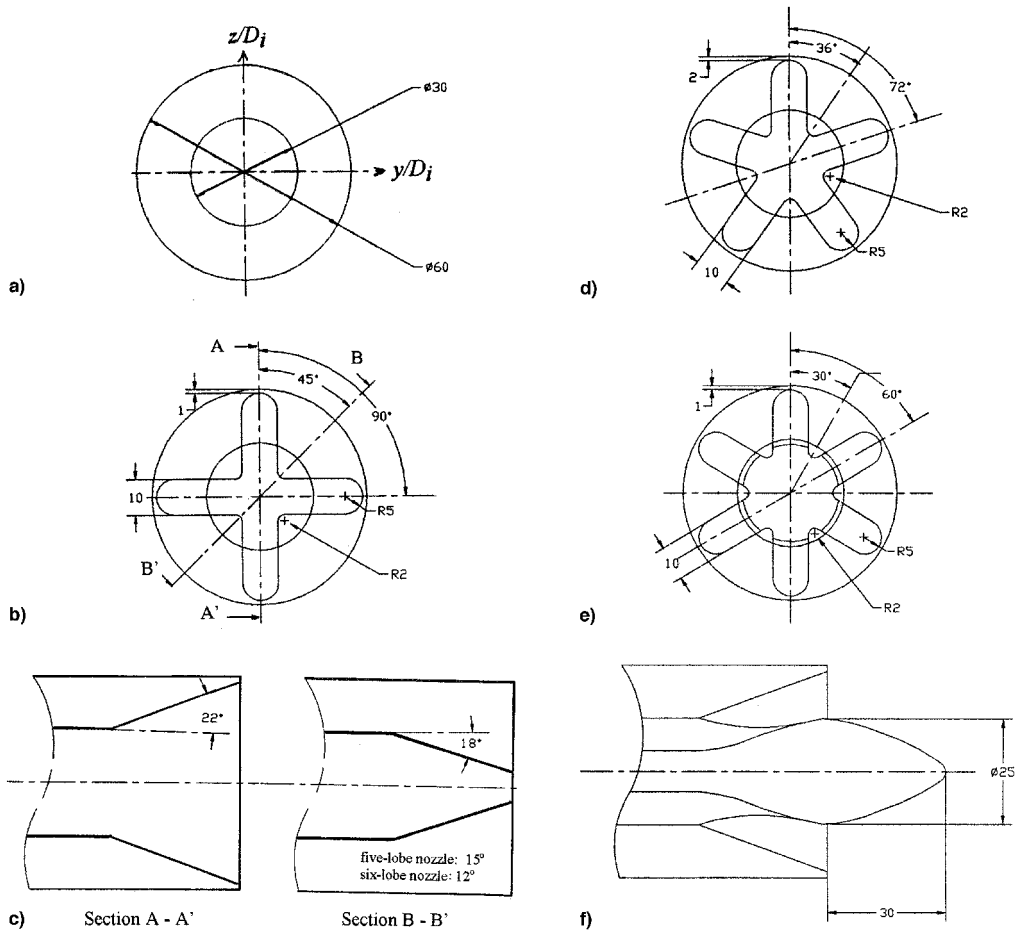

Fig. 3 Dimensions of the coaxial nozzles considered (all dimensions in millimeters; thickness of the walls = 1.5 mm).

dimensions of each nozzle configuration. The coaxial circular nozzle is intended to be used as a baseline reference case where the generation of streamwise vorticity is not expected. Preliminary experiments were performed on this configuration to ensure the reproducibility of previously published results in the present rig. Nozzle 2 has four lobes and nozzles 3 and 4 have five and six lobes, respectively. The penetration angle from the annular side to the core is kept at 22 deg. To maintain the straight parallel sidewalls at each lobe for all cases, the area of the central nozzle at the exit plane increases with the number of lobes: 1057 m^2 for four lobes, 1218 m^2 for five lobes, and 1335 m^2 for six lobes. As a consequence of the change in the central lobe area the penetration angle from the core to the annular varies with the number of lobes: 18 deg for the four lobes, 15 deg for the five lobes, and 12 deg for the six lobes. For all cases considered, the outer nozzle has a diameter of 60 mm. There is also a small gap of 1 mm (2 mm for the five-lobed case) between the peaks of each lobe and the inner wall of the outer nozzle.

For the six-lobed nozzle, a central plug was introduced to determine its effectiveness on mixing after streamwise flow separation had been detected at the nozzle exit plane and at the peaks of each lobe. The detailed dimensions of the plug are provided in Fig. 3f.

C. LDA

A four-beam, two-component fiber-optic LDA with a 300-mW argon air-cooled laser operating in a backward-scattered mode was used to measure velocity measurements. A focusing lens of 400 mm provided a measuring probe volume of 0.09 × 0.09 × 1.31 mm in the vertical direction z, and 0.085 × 0.085 × 1.24 mm in the streamwise direction x. The fiber-optic probe was mounted on an automated three-dimensional traversing system with an accuracy of ±0.01 mm. Bragg shifting with a frequency up to 2 MHz (on each channel) was used to avoid directional ambiguity. The Doppler signals were detected by photomultipliers and processed by the automatic burst correlators (IFA 750). The natural contaminants inside the water appears to be sufficient to produce a high validation data rate. Except at some regions immediately behind the trailing edge, data rates of 500–1000 Hz were normally obtainable. At each measuring point, the mean velocities, the rms of the velocity fluctuations, and the Reynolds shear stresses were determined from populations of more than 5000 samples (on each channel), together with a coincidence window of 1 μs.

A detailed evaluation on the errors associated with the LDA system was conducted. The sources of error stemmed mainly from velocity biasing,[13] velocity gradient broadening,[14] the accuracy of the signal processor, and the finite sampling size.[15] Thus, the accuracy of the measured velocity components (normalized by the bulk mean velocity of the two streams U_r 1.7 m/s) can be expected to be about 1% and that of the rms of the velocity fluctuations (normalized by U_r) and the Reynolds shear stresses (normalized by U_r^2) to be 3%, based on a 95% confidence level.

Measurements of the three-orthogonal mean velocities (U, V_r, V_θ), their corresponding rms fluctuations (u', v_r', v_θ'), and Reynolds shear stresses ($\overline{u'v_r'}$, $\overline{u'v_\theta'}$ only) were acquired in the projected area corresponding to one lobe as shown in Fig. 2a, and at downstream locations of x/D_i = 0.25, 0.5, 1, 2, 3, 4, 5, and 6. At each station, there were about 400 (at stations near the jet exit) to 900 (far downstream) measuring points at each lobe. Symmetry of the flow about the horizontal y and vertical z axes at the exit plane of the jet was within 5%, based on the calculations of the mass flux uniformity. The streamwise component of the vorticity [$\Omega_x = (\partial V_r/r\partial\theta) - (\partial V_\theta/\partial r)$] was cal-

Table 1 Characteristics of exit boundary layers[a]

Boundary-layer parameter	Inner jet	Annular jet	
		Inner	Outer
δ^*, cm	0.5	0.43	0.43
Θ, cm	0.27	0.24	0.25
H	1.85	1.79	1.72
Re_Θ	303.3	569.6	593.3

[a]Coaxial nozzle configuration.

culated based on a third-order polynomial fit to the V_θ and V_r measurements.

D. Initial Conditions

The distribution of the streamwise mean velocity along the y and z directions measured at $x/D_i = 0.05$ for the coaxial nozzle are shown in Table 1. Both boundary-layer parameters and boundary-layer profiles indicated that the boundary layers on every wall of the coaxial nozzle were turbulent. The initial conditions produced here were the same as those used in Ref. 16. Streamwise turbulence levels outside the boundary-layer region at the core and the annular had maximum values of 1.0 and 1.2%, respectively (normalized by the mean velocity of the two streams).

III. Results and Discussion

Downstream development for the streamwise mean velocities, streamwise mean vorticity, and turbulent kinetic energy are presented as either isocontours while the secondary mean flow velocities are presented as vectors (where the arrow base indicated the measuring point). Because of limited space, only the most representative results are shown in this paper. The detailed results can be found in Ref. 12.

A. Centerline Mean Velocities

Figure 4 shows the centerline distribution of the streamwise mean velocity (normalized by the mean velocity of the two streams) for the four cases considered. The six-lobed nozzle case with the center plug is shown in Fig. 4b. A sudden reduction for the streamwise mean velocity is characterized by all nozzle configurations in the first diameter downstream of the nozzle exit plane with the four-lobed nozzle reduced at the fastest rate. This reduction is largely a result of the increase in the central-lobed nozzle cross-sectional area when compared to a coaxial jet.

The initial values at the exit plane are slightly different for all of the cases and can be attributed to the increase in the cross-sectional area as the number of lobes increases. After $x/D_i = 1$, the annular flow starts to influence the mean velocity at the centerline, which shows an increase in magnitude for all of the lobed nozzle cases, with the highest growth rate for the five-lobed nozzle. The growth rate is mainly influenced by the strength of the streamwise vortices shed by the lobes. The centerline velocity reaches a peak at $x/D_i = 2.75$ for the five-lobed nozzle, at $x/D_i = 5.0$ for the four-lobed nozzle, and at $x/D_i = 6.0$ for the six-lobed nozzle. Unlike those found in the lobed nozzle cases, the centerline variation for the baseline nozzle after $x/D_i = 1.0$ appears to undergo two stages: 1) a low-growth-rate region between $x/D_i = 1.0$–4.0 and 2) a high-growth-rate region from $x/D_i = 4.0$ when the velocity reaches a maximum at about $x/D_i = 8.0$.

The centerline velocity variation in the baseline configuration can be classified into three zones: 1) the initial merging zone (from the trailing edge to $x/D_i = 1.0$), 2) the intermediate zone (between $x/D_i = 1.0$–4.0), and 3) the fully merged zone (beyond $x/D_i = 4.0$).[4] All of the lobed nozzle cases showed that the slow-growing intermediate zone, where the spanwise vorticity begins to entrain the annular fluid toward the centerline, is not present. Thus, the comparison in Fig. 4 highlights

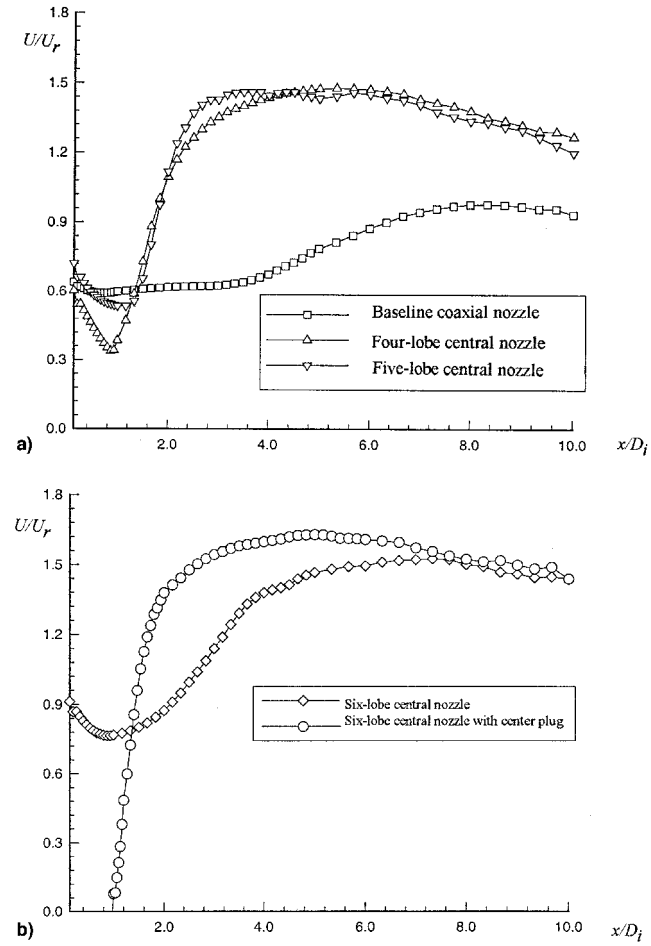

Fig. 4 Variation of the centerline velocities for respective coaxial nozzles.

the fact that streamwise vorticity is more efficient in convecting the high-momentum annular fluid to the nozzle centerline than by the spanwise vorticity alone.

A central plug was introduced after streamwise separation was detected at the lobe peaks for the six-lobed nozzle. This separation is primarily because of the excessive increase in the central-lobed nozzle cross-sectional area. Subsequent measurements around the lobed peak regions did not reveal further streamwise flow separations. The location of maximum velocity is also seen to shift further upstream to the trailing edge, suggesting an improvement to the mixing process between the coflowing streams (Fig. 4b).

B. Downstream Development of the Streamwise and Secondary Mean Velocities

Since the flow development for the four-, five- and six-lobed cases are very similar to each other, only the results for the six-lobed case are shown here.

Contours of the streamwise mean velocity and the corresponding secondary flow velocity vectors at four selective downstream locations from the exit plane are presented in Fig. 5. A pair of counter-rotating vortices are formed immediately downstream at the trailing edge at $x/D_i = 0.5$ for the four- and five-lobed configurations, with the vortex core located around the midpoint of the straight parallel sidewall. For the six-lobed case, two pairs of vortices are formed (Fig. 5a). The extent of the outward radial flow from the central nozzle reached the peak of each lobe in the four- and five-lobed cases, whereas for the six-lobed case regions of streamwise separation appeared at the lobe peaks. The strength of the secondary flow velocities, in general, is found to be higher at the annular (inward radial direction) region than (in the outward radial direc-

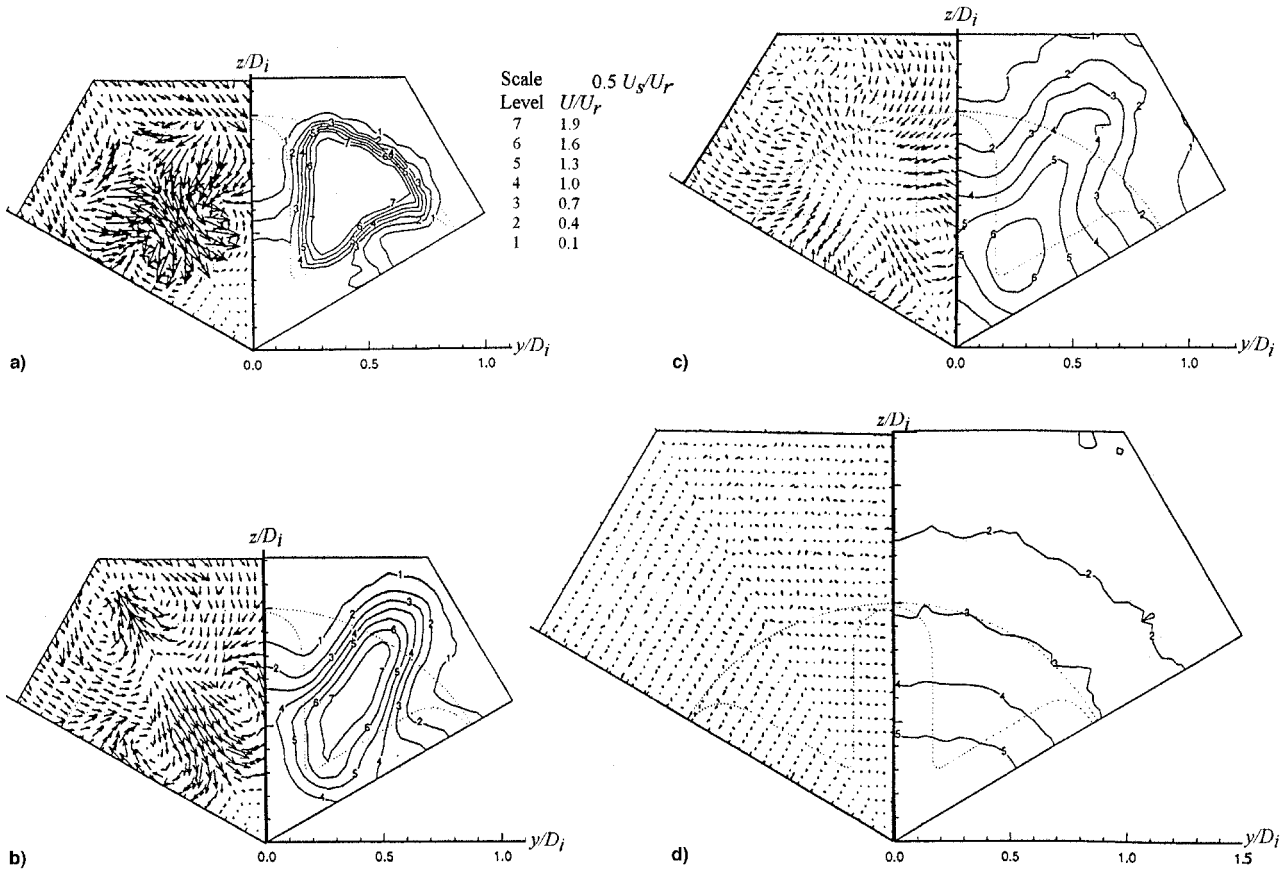

Fig. 5 Contours of the normalized streamwise velocity U/U_r and the corresponding secondary flow velocity vectors U_s/U_r at successive stations downstream of the trailing edge: six-lobed central nozzle.

tion) along the lobes; the six-lobed case has the highest strength with a maximum of about $0.5U_r$, compared to a maximum of $0.35U_r$ for the four- and five-lobed cases. The secondary flow pattern at the separation regions for the six-lobed case essentially consisted of velocity vectors directed toward the annular region. It appears that the flow separation has facilitated the inward radial flow from the surrounding area toward the annular region.

From $x/D_i = 1.0$ onward (Fig. 5b), streamwise mean velocity contours at the annular wall region begin to shift radically outward to the surrounding area in the direction along the plane of symmetry and is more discernible in the six-lobed case largely because of a smaller gap between lobe peaks and the inner annular wall. The migration becomes more significant so that by $x/D_i = 2.0$ (Fig. 5c) the stretching of the contour lines along the line of symmetry had actually penetrated substantially (and diffused) into the surrounding area. Subsequent examination of the corresponding secondary velocity vector plots revealed that this radial migration originated from the radial flow discharged from the gap between the lobe peaks and the inner annular wall. The same characteristic prevailed in all of the lobed-nozzle cases considered here, but not in the measurements of Belovich and Samimy.[6] In Belovich and Samimy's case,[6] the gap between the central-lobed nozzle and the annular jet was of the order of the inner diameter.

Because of limited optical access, measurements cannot be obtained upstream of the trailing edge. Based on the previous visualization studies by the authors on a two-dimensional lobed mixer,[17] the flow approaching the lobe peaks would be decelerated and deflected sideways as a result of the high-pressure buildup at the peak region (Fig. 6). It is therefore conceivable that the flow was pushed through the small gap between the lobe peak and the inner annular wall to provide this outward radial movement.

By $x/D_i = 4.0$ (Fig. 5d), the strength of the secondary flow velocity had been reduced substantially and the corresponding streamwise mean velocity distribution became more axisymmetric. Beyond $x/D_i = 6$, the secondary flow velocity for all of the cases considered had been reduced to a negligible level, whereas the corresponding streamwise mean velocity contours had shown an approach more like that of a single jet.

Integration of data similar to those shown in Fig. 5 provided the mass flux at different streamwise locations. These data are shown in Fig. 7 and clearly demonstrated the increased entrainment caused by the central-lobed nozzle. In contrast to those observed in the centerline distribution (Fig. 4a), the six-lobed case was lower initially, but became higher and eventually overtook the other cases after $x/D_i = 2.0$. This observation implies that the number of lobes has basically a dominant effect to the overall mixing processes. The growth rate for all of the cases begins to drop after $x/D_i = 5.0$ largely because of streamwise vorticity dissipation. The mass flux entrainment, in the presence of the streamwise vorticity, was some 30% higher than the baseline coaxial nozzle. However, it can be expected that the difference would be smaller if the streamwise vorticity generated by the gap was absent, as shown in the measurements of Belovich and Samimy.[6] The growth rate of the mass flux entrainment for the six-lobed case with the center plug was found to be higher only in the first diameter when compared to that without the center plug. The overall increase in mass flux is still lower than that of the case without the plug. The plug is effective in reducing the flow separation at the peaks, but in turn it suppressed the streamwise vorticity generated by the gap and, hence, led to a lower increase in mass flux entrainment. It should also be noted that while the velocity along the centerline can provide some information on the mixing effectiveness between two coflowing streams, the mass flux calculation can provide information on

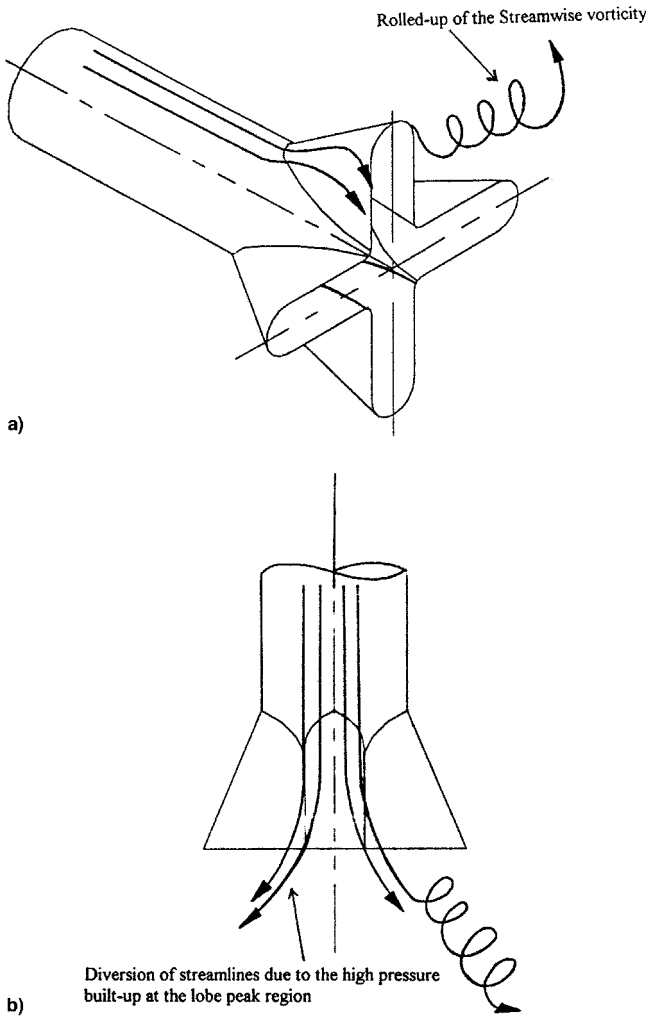

Fig. 6 Schematic of the flow in the vicinity of the lobed peak region.

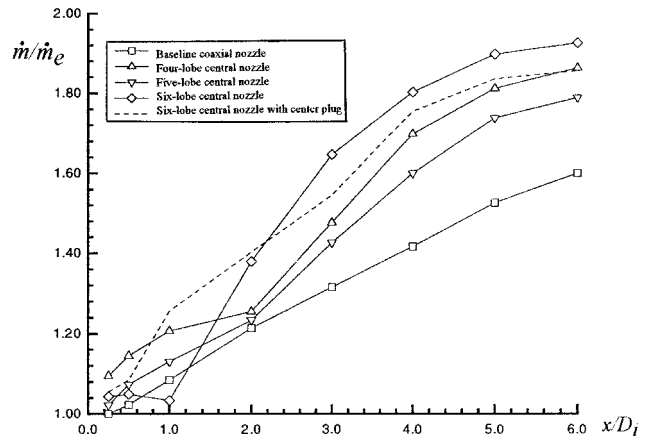

Fig. 7 Streamwise variation of the normalized mass flux.

the overall mixing process, particularly with the surrounding still fluid.

The gap between the central nozzle peaks and the inner annular wall is important to the generation of streamwise vorticity. Subsequent investigations were conducted to examine the effects on the distance of the gap by varying systematically the diameter of the outer annular nozzle for the five-lobed case. Altogether, five gap distances were tested including $0.0D_i$ (i.e., no gap), 0.05, 0.1, 0.15, and $0.2D_i$. For each case, measurements were only obtained at station $x/D_i = 1.0$. The most optimum gap distance appeared to be within the range of 0.05–$0.1D_i$. It was found that when the gap was above $0.15D_i$, the stretching of the contours along the plane of symmetry would become unnoticeable and less significant when the gap was filled.

C. Downstream Development of the Mean Streamwise Vorticity

The mean streamwise vorticity contours at selective streamwise locations for the six-lobed are presented in Fig. 8. As may be expected, two symmetrical pairs of counter-rotating streamwise vortices are formed behind the trailing edge at $x/D_i = 0.25$ and Fig. 8a for the six-lobed case. The size and

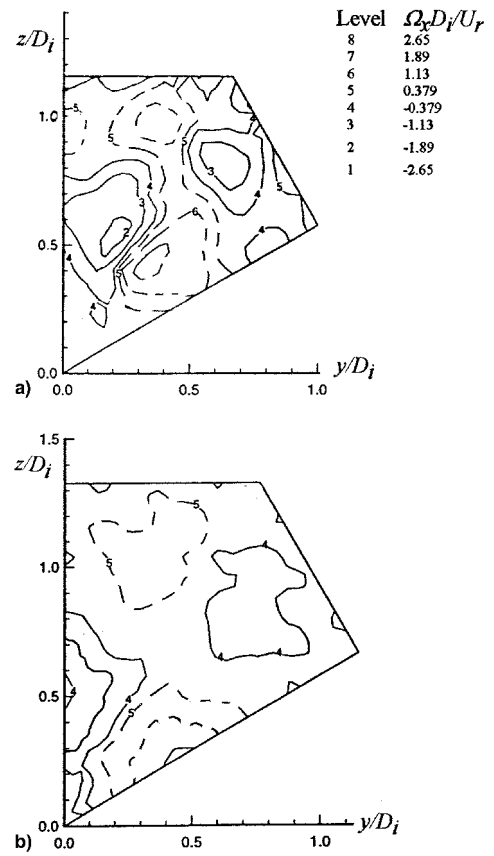

Fig. 8 Contours of the normalized streamwise mean vorticity $\Omega_x D_i/U_r$ at successive stations downstream of the trailing edge: six-lobed central nozzle.

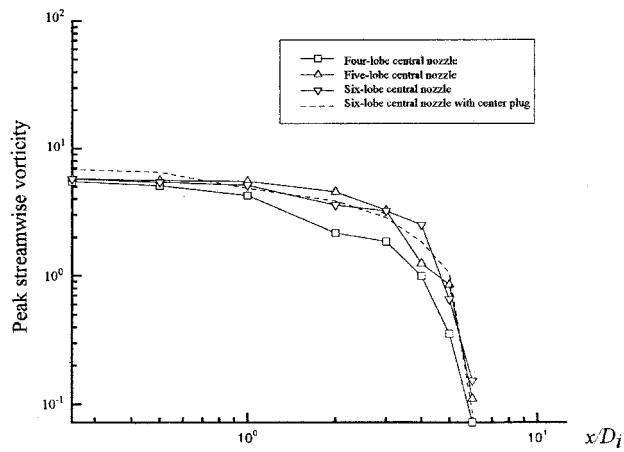

Fig. 9 Streamwise variation of the normalized peak streamwise vorticity.

strength of the vortices shed by the lobe is nearly the same as those that appeared near the annular wall. The mean streamwise vorticity for both cases maintains nearly the same strength from the trailing edge to about $x/D_i = 2.0$ (see Fig. 8b). After $x/D_i = 2.0$ and to the end of the measurement range, the mean streamwise vorticity strength decreases rapidly.

The development of the peak mean streamwise vorticity in Fig. 9 is plotted on a log–log scale. Results for all of the cases here appear to fall on the same decaying curve within the range of measurement. It should be noted that the average circulation (not shown here) had actual decay faster than that of the peak vorticity. The breakdown of the large-scale vortices into smaller (but not weaker) vortices caused mixing at a finer scale.

D. Downstream Development of the Reynolds Shear Stresses and Turbulent Kinetic Energy

The distribution of the other turbulence quantities in the wake are also affected by the presence of the streamwise vorticity. Since the effects on all of the Reynolds stresses for all of the lobed nozzle cases were quantitatively similar, only the $\overline{uv}_r/U_r^2$ and the turbulent kinetic energy k/U_r^2 for the six-lobed nozzle are presented in Figs. 10 and 11, respectively. At $x/D_i = 0.5$ and Fig. 10a local peaks of both signs are observed. The distribution of the Reynolds shear stresses closely follows the distribution of the streamwise mean velocity contours at the subsequent station (Fig. 10b); the peaks are generally located at regions of high mean shear that lead to high production [through the $v_r^2(\partial U/\partial r)$ term in the $\overline{uv}_r$ transport equations]. After $x/D_i = 4.0$, the level of the Reynolds shear stresses reduced after the smoothing out of the steep velocity gradients.

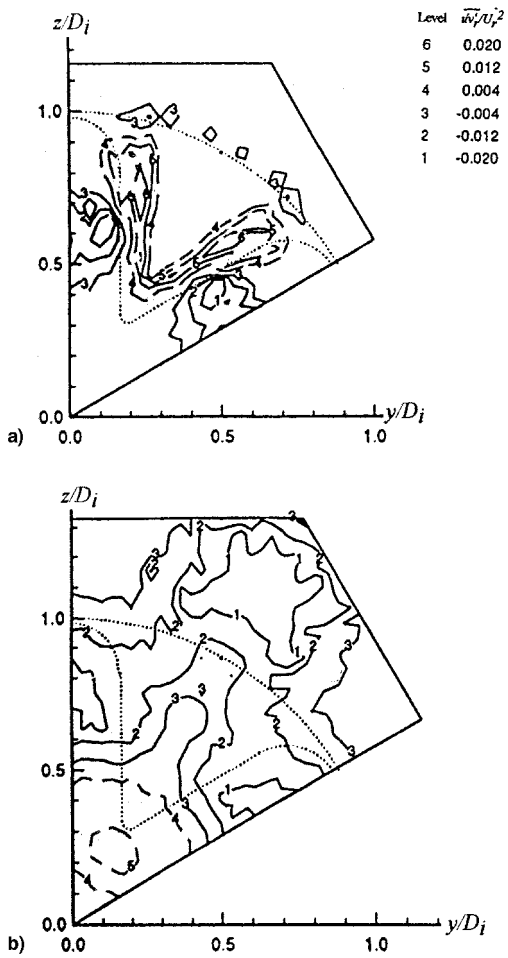

Fig. 10 Contours of the normalized Reynolds shear stress ($\overline{uv}_r/U_r^2$) at successive downstream stations of the trailing edge: six-lobed central nozzle.

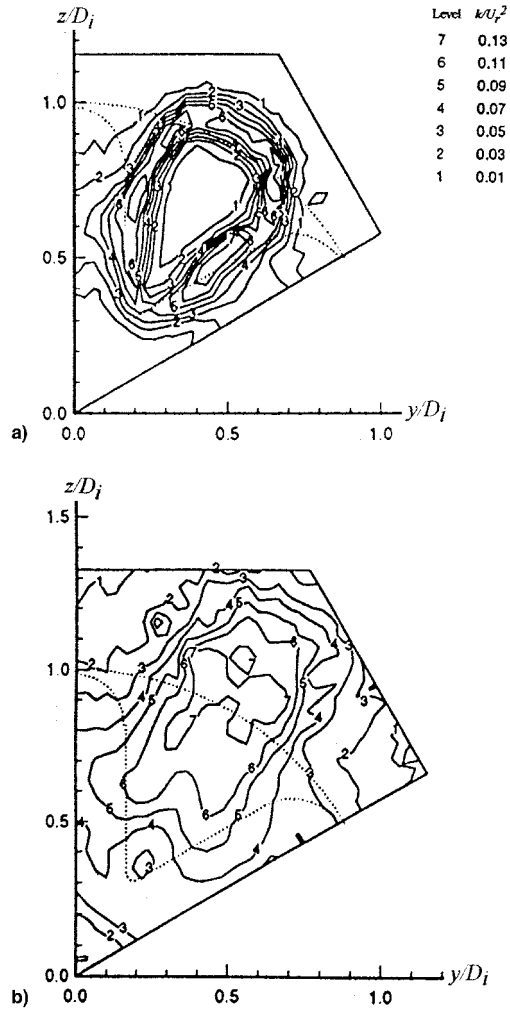

Fig. 11 Contours of the normalized turbulent kinetic energy (k/U_r^2) at successive downstream stations of the trailing edge: six-lobed central nozzle.

The downstream development of turbulent kinetic energy k/U_r^2 for the six-lobed nozzle are presented in Fig. 11. A higher level of k appeared initially at the wake of the walls immediately downstream of the trailing edge at $x/D_i = 0.5$ and Fig. 11a. As a consequence of the streamwise vorticity shed by the lobes, higher k-level regions appear and subsequently begin to diffuse around the straight parallel sidewall of each lobe (the pinched-off effects as described by McCormick et al.[7]). Further downstream at about $x/D_i = 1.0–2.0$ and Fig. 11b, additional production of k appears at the locations near the plane of symmetry (may be termed as the second pinched-off effects). It should be noted that the support for the production of the turbulent kinetic energy at the first pinched-off location is mainly through the $\overline{uv}_r(\partial U/\partial r)$ term in the turbulent kinetic energy transport equations, whereas for the second pinched-off location, the $\overline{uv}_\theta(\partial U/r\partial\theta)$ term appears to be more important. By the end of the measurement range, the levels of k across the wake in general are higher than those at the locations close to the trailing edge.

IV. Concluding Remarks

The mixing characteristics of turbulent, confined, coaxial-flow jets with a central-lobed mixer have been measured using a two-component fiber-optic LDA with initial turbulent boundary layers at the velocity ratio 2:1 (outer to inner). Altogether, three central-lobed mixer configurations were tested, including

four-, five- and six-lobed nozzles. A center plug was also used in the six-lobed case after flow separations were detected at the lobed peak regions.

In addition to the generation of the streamwise vorticity that one would expect from the geometry of the lobe, streamwise vorticity was also found to originate between the lobed peaks and the inner annular walls. It is obvious that the former is important to enhance the mixing between the two coflowing streams, whereas the latter is important to the mixing between the annular flow and the surrounding still fluid. It was also found that when the gap was above $0.15D_i$, no streamwise vorticity would be generated. The streamwise vorticity generated by the gap could be further strengthened by the streamwise separation that occurred at the lobe peaks. It was conceivable that without the presence of the streamwise vorticity generated by the gap, the mass flux entrainment may not be as significant. Studies showed that the area of spread for a six-lobed central nozzle was only about 10% higher than the baseline circular nozzle. In the present case, despite being in a confined environment, a 30% increase was observed for the six-lobed nozzle compared to that of the baseline coaxial nozzle.

As may be expected, in the presence of streamwise vorticity generated by the geometry of the lobe, the flow between the two coflowing streams can actually mix faster than the normal coaxial nozzle arrangement and the number of the lobes at the central nozzle played a crucial role in the mixing process. The average circulation for each streamwise vortex actually decayed faster than that of the peak vorticity. This implies that during the breakdown of the large-scale vortices, smaller, but not weaker, vortices would be formed, which in turn causes finer-scale mixing to be achieved.

The introduction of the center plug in the six-lobed case forced the flow through the lobe penetration region and thereby reduced the onset of flow separation at the peaks. The plug is therefore found to be beneficial to the mixing between the two coflowing streams (as shown in the centerline velocity measurements), but not to the overall mass flux entrainment caused by the suppression of the streamwise vorticity generated by the gap.

Of particular note is that there were two occasions where high-turbulent kinetic energy was being generated. The first was within the lobe after the pinched-off effect appeared, and subsequently, at a slightly downstream location where the annular flow was being stretched along the plane of symmetry to the surrounding area by the streamwise vorticity generated by the gap. At both instances, streamwise vorticity played an important role to the generation of the turbulent kinetic energy. It is again obvious that the turbulent kinetic energy generated at the first pinched-off location is responsible for the fine mixing between the two coflowing streams, whereas that at the second pinched-off location is responsible for the fine mixing between the annular flow and the surrounding still fluid.

Acknowledgment

The authors are grateful to the Academic Research Grant Committee for the financial support to this project.

References

[1]Ribeiro, M. M., and Whitelaw, J. H., "Turbulent Mixing of Coaxial Jets with Particular Reference to the Near-Exit Region," *Journal of Fluids Engineering*, Vol. 98, 1976, pp. 284–291.

[2]Ribeiro, M. M., and Whitelaw, J. H., "Coaxial Jets with and Without Swirl," *Journal of Fluid Mechanics*, Vol. 96, No. 4, 1980, pp. 769–795.

[3]Champagne, F. H., and Wygnanski, I. J., "An Experimental Investigation of Coaxial Turbulent Jets," *International Journal of Heat and Mass Transfer*, Vol. 14, 1971, pp. 1445–1464.

[4]Ko, N. W. M., and Kwan A. S. H., "The Initial Region of Subsonic Coaxial Jets," *Journal of Fluid Mechanics*, Vol. 73, 1976, pp. 305–332.

[5]Kwan, A. S. A., and Ko, N. W. M., "The Initial Region of Subsonic Coaxial Jets," *Journal of Fluid Mechanics*, Vol. 82, Pt. 2, 1977, pp. 273–287.

[6]Werle, M. J., Paterson, R. W., and Presz, W. M., Jr., "Flow Structure in a Periodic Axial Vortex Array," AIAA Paper 87-0610, Jan. 1987.

[7]McCormick, D. C., and Bennett, J. C., Jr., "Vortical and Turbulent Structure of a Lobed Forced Mixer Free-Shear Layer," *AIAA Journal*, Vol. 32, No. 9, 1994, pp. 1852–1859.

[8]Yu, S. C. M., and Yip, T. H. "Measurements of Velocities in the Near-Field of a Lobed Forced Mixer Trailing Edge," *Aeronautical Journal of the Royal Aeronautical Society*, Vol. 101, March 1997, pp. 121–129.

[9]Yu, S. C. M., Xu, X. G., and Yip, T. H., "Effects of Initial Boundary Layers to the Lobed Mixer Trailing Streamwise Vorticity," *Journal of Propulsion and Power*, Vol. 12, No. 2, 1996, pp. 440–442.

[10]Belovich, V. M., and Samimy, M., "Mixing Processes in a Coaxial Geometry with a Central Lobed Mixer Nozzle," AIAA Paper 96-0118, June 1996.

[11]Yu, S. C. M., and Xu, X. G., "Vortical Structure of Coaxial Nozzle Flow with a Central Lobed Mixer at Different Velocity Ratios," AIAA Paper 97-1811, June 1997.

[12]Xu, X. G., "Measurements of Co-Axial Nozzles with a Central Lobed Mixer," M.S. Thesis, School of Mechanical and Production Engineering, Thermal and Fluids Engineering Div., Nanyang Technological Univ., Singapore, 1996.

[13]Durao, D. F. G., Laker, J., and Whitelaw, J. H. "Bias Effects in Laser-Doppler Anemometry," *Journal of Physics E: Scientific Instruments*, Vol. 13, 1979, p. 442.

[14]Durst, F., Melling, A., and Whitelaw, J. H., *Principles and Practice of Laser-Doppler Anemometry*, Academic, London, 1981.

[15]Yanta, W. J., and Smith, R. A., "Measurements of Turbulence Transport Properties with a Laser-Doppler Velocimeter," AIAA Paper 73-169, 1973.

[16]Buresti, G., Talamelli, A., and Petagna, P., "Experimental Characterization of the Velocity Field of a Coaxial Jet Configuration," *Experimental Thermal and Fluid Science*, Vol. 9, 1994, pp. 135–146.

[17]Yu, S. C. M., Yip, T. H., and Liu, C. Y., "Mixing Characteristics of Forced Mixers with Scalloped Lobes," *Journal of Propulsion and Power*, Vol. 13, No. 2, 1997, pp. 305–311.